Striped dilute liquid of dipolar bosons in two dimensions

Clemens Staudinger,[1] Diana Hufnagl,[2,3] Ferran Mazzanti,[4] and Robert E. Zillich[1]
[1]*Institute for Theoretical Physics, Johannes Kepler University, Altenbergerstrasse 69, 4040 Linz, Austria*
[2]*Johann Radon Institute for Computational and Applied Mathematics, Austrian Academy of Sciences, Altenberger Straße 69, 4040 Linz, Austria*
[3]*MathConsult GmbH, Altenbergerstrasse 69, 4040 Linz, Austria*
[4]*Departament de Física, Campus Nord B4-B5, Universitat Politècnica de Catalunya, E-08034 Barcelona, Spain*

(Received 21 March 2023; accepted 11 August 2023; published 5 September 2023)

We investigate the phases of a Bose-Einstein condensate of dipolar atoms restricted to move in a two-dimensional plane. The dipole moments are all aligned in a direction tilted with respect to the plane normal. As a result of the attractive and repulsive components of the dipole-dipole interaction, the dipolar gas has a self-bound phase, which is stabilized by quantum fluctuations. Tilting the dipoles tunes the anisotropy of the dipole-dipole interaction, which can trigger a spatial density modulation. In this work we study these two aspects and investigate the conditions for the formation of a self-bound and striped phase, which has been realized in experiments with dipolar droplets. We use a variational method based on the hypernetted-chain Euler-Lagrange optimization of a Jastrow-Feenberg ansatz for the many-body wave function to study the ground-state properties. This method takes into account quantum fluctuations in a nonperturbative way and thus can be used also for strongly correlated systems.

DOI: 10.1103/PhysRevA.108.033303

I. INTRODUCTION

Dipolar quantum gases, and especially dipolar Bose-Einstein condensates (BEC), are gaining significant attention [1] since self-bound droplets consisting of ^{164}Dy [2–7] and ^{166}Er [8] were realized in experiments. In contrast to Bose mixtures, the competition between attractive and repulsive parts of the interaction does not originate from the interaction between the components of the mixture, but rather from the dipole-dipole interaction itself, which in general has repulsive and attractive regions. Quantum fluctuations have been recognized as being important for dipolar quantum gases [9,10]. Particularly, as in Bose mixtures' droplets [11–14], quantum fluctuations are the driving force behind the stabilization of dipolar droplets, as confirmed by theory [15–17]. More recently, dipolar mixtures have been realized in experiments [18,19] and the properties of self-bound droplets of these mixtures have been described with beyond mean-field methods [20,21]. In such droplets the components are not necessarily miscible, but can demix while staying self-bound.

In experiments the dipole moments of all atoms are aligned in parallel by an external magnetic field of well-controlled strength and direction. This provides a means to modify the anisotropy of the dipole-dipole interaction and triggers the transition to a density-modulated, self-organized stripe phase, which shows supersolid properties [22–27]. Such a transition is also visible in the excitation spectrum of a dipolar BEC, where a so-called roton minimum emerges [28–33]. Just like a droplet, a density modulation is a state that is not stable in a mean-field approximation [34,35], but rather is stabilized by quantum fluctuations [36].

In previous theoretical studies [37], we observed density modulations in the form of stripes in a two-dimensional dipolar Bose gas with the polarization axis tilted with respect to the perpendicular direction. In these studies, where the tilt angle θ was small enough that the dipole interaction stayed purely repulsive, a very high density was required to reach the stripe phase, and no self-binding was involved. In this work, we investigate the formation of stripes at much lower densities which can be realized in experiments with magnetic dipole moments. We achieve this by increasing the tilting angle θ beyond a critical angle, where the projection of the dipole-dipole interaction on the two-dimensional (2D) plane becomes attractive (see Fig. 1), such that self-binding is possible. Density oscillations have been observed experimentally [38–41]. Conventional mean-field theories are not capable of describing such situations, and more powerful methods like extended mean-field with Lee-Huang-Yang corrections [5,8] or quantum Monte Carlo (QMC) techniques [17,42–45] have to be applied. In this work, we employ the hypernetted-chain Euler-Lagrange (HNC-EL) method [46–48], which incorporates correlations necessary to describe strongly correlated and self-bound systems [49,50], but requires a much lower computational effort than QMC techniques.

II. METHODOLOGY

In the following we consider a dipolar Bose gas that is so tightly trapped in the z direction that we can assume particles are restricted to move in two dimensions, taken to be the xy plane. The Hamiltonian reads

$$\hat{H} = -\frac{\hbar^2}{2m}\sum_{i=1}^{N}\Delta_i + \sum_{i<j} v(\boldsymbol{r}_i - \boldsymbol{r}_j), \tag{1}$$

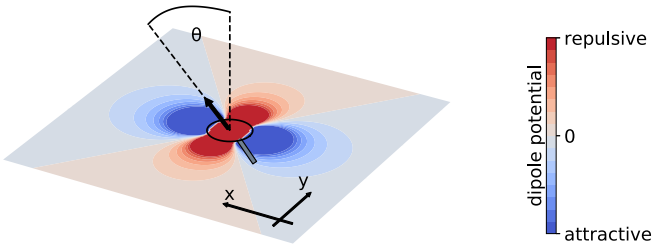

FIG. 1. Sketch of the dipolar interaction in 2D, with the tilting angle θ and the repulsion parameter $C_{\rm h}$. The direction of the dipole moment is shown by the black arrow and the repulsion is indicated by the black circle. The compound interaction leads to a repulsive region along the y direction and an attractive region along the x direction, shown in red and blue, respectively.

with the interaction being the sum of the dipolar term and a respulsive core,

$$v(\boldsymbol{r}) = \frac{C_{dd}}{4\pi}\left[\frac{1}{|\boldsymbol{r}|^3} - \frac{3(x\sin\theta)^2}{|\boldsymbol{r}|^5}\right] + \frac{E_0 C_{\rm h}^{12}}{|\boldsymbol{r}|^{12}}. \tag{2}$$

In this expression C_{dd} sets the strength of the dipolar interaction and is proportional to the square of the (electric or magnetic) dipole moment. It is useful to define the characteristic length scale $r_0 = mC_{dd}/(4\pi\hbar^2)$ and the associated energy scale $E_0 = \hbar^2/(mr_0^2)$, which serve as units for our calculations. All dipoles are polarized along a direction in the xz plane that forms an angle θ with respect to the z axis (see Fig. 1). With this geometry, the dipole-dipole interaction is repulsive around the y direction (red regions in Fig. 1), but for large enough $\theta > \theta_{\rm c} = \arcsin(1/\sqrt{3}) \approx 0.615\,48$ an attractive region appears in the x direction (blue regions in Fig. 1). In this work we explore the highly tilted polarization regime $\theta > \theta_{\rm c}$ where the purely dipolar gas is unstable. In order to prevent collapse, we add a short-range repulsive interaction $1/r^{12}$ potential with the short-range repulsion parameter $C_{\rm h}$ as shown in Eq. (2). As a check of universality of this model, we compare the results with those obtained with a $1/r^6$ potential tuned to the same total scattering length.

We describe the ground state using a variational Jastrow-Feenberg ansatz [51] of the form

$$\Psi(\boldsymbol{r}_1,\ldots,\boldsymbol{r}_N) = \exp\left[\frac{1}{2}\sum_{i=1}^{N} u_1(\boldsymbol{r}_i) + \frac{1}{2}\sum_{i<j} u(\boldsymbol{r}_i - \boldsymbol{r}_j)\right]. \tag{3}$$

The one-body functions $u_1(\boldsymbol{r}_i)$ are necessary if the system is not uniform; since we restrict ourselves to a homogeneous Bose gas, we can set $u_1(\boldsymbol{r}_i) \equiv 0$. $u(\boldsymbol{r}_i - \boldsymbol{r}_j)$ are pair correlations which do not vanish since the Hamiltonian (1) contains interactions v. If $u(\boldsymbol{r}_i - \boldsymbol{r}_j) = 0$, Ψ reduces to the Hartree wave function, i.e., the mean-field approximation. In this sense, pair (and possibly higher-order) correlations generate quantum fluctuations, but nonperturbatively; i.e., we do not need to assume the corrections to mean field are small.

In order to obtain the optimal ground state, we solve the Euler-Lagrange equation

$$\frac{\delta e}{\delta\sqrt{g(\boldsymbol{r})}} = 0, \tag{4}$$

where e is the energy per particle,

$$e(\rho_0) \equiv \frac{E}{N} = \frac{\rho_0}{2}\int d^2r\, g(\boldsymbol{r})\left[v(\boldsymbol{r}) - \frac{\hbar^2}{4m}\nabla^2 u(\boldsymbol{r})\right]. \tag{5}$$

The pair distribution function $g(\boldsymbol{r})$ is given in terms of the wave function in Eq. (3) as

$$g(\boldsymbol{r}_1 - \boldsymbol{r}_2) = \frac{N(N-1)}{\langle\Psi|\Psi\rangle\rho_0^2}\int d^2r_3\ldots d^2r_N|\Psi(\boldsymbol{r}_1,\ldots,\boldsymbol{r}_N)|^2. \tag{6}$$

Closure is provided by the HNC relation between $g(\boldsymbol{r})$ and $u(\boldsymbol{r})$ [52]. In the following, we restrict ourselves to the HNC-EL/0 approximation, where the so-called elementary diagrams are neglected in the cluster expansion [52]. We have calculated the leading contribution of the elementary diagrams to the total energy but found it to be less than 3% for densities $\rho_0 r_0^2 \leqslant 1$ (see Appendix C). In the HNC-EL/0 framework, Eq. (4) can be cast as

$$\left[-\frac{\hbar^2}{m}\Delta + v(\boldsymbol{r}) + w_{\rm I}(\boldsymbol{r})\right]\sqrt{g(\boldsymbol{r})} = 0, \tag{7}$$

which has the form of an effective two-body zero-energy scattering equation with the bare potential v and an additional induced many-body potential $w_{\rm I}$, which is defined via its Fourier transform

$$w_{\rm I}(\boldsymbol{k}) = -\frac{\hbar^2k^2}{4m}\left(1 - \frac{1}{S(\boldsymbol{k})}\right)^2[2S(\boldsymbol{k}) + 1]$$

in terms of the static structure factor

$$S(\boldsymbol{k}) = 1 + \mathrm{FT}[g(\boldsymbol{r}) - 1], \tag{8}$$

where FT denotes the Fourier transformation multiplied with the density ρ_0. We note that Eq. (7) is not a simple linear differential equation because the induced potential $w_{\rm I}$ depends on g itself. The details on how to solve Eq. (7) iteratively can be found elsewhere [47,48].

From experience with other systems [49,50,53–55], solving the HNC-EL/0 equations is straightforward for systems with a stable or metastable ground state, but fails to converge if the system is unstable against infinitesimal perturbations (e.g., spinodal instability of a system with homogeneous density [50,54]). Inspection of structural quantities like $g(\boldsymbol{r})$ and $S(\boldsymbol{k})$ provides clues as to the nature of the instability (e.g., long-ranged oscillations in $g(\boldsymbol{r})$ in the case of a spinodal instability). More quantitative information on that is provided by a stability analysis of the solution of the HNC-EL/0 equation [56]. For this purpose, we evaluate the Hessian, i.e., the second functional derivative of the energy e with respect to the pair distribution function, $K(\boldsymbol{r},\boldsymbol{r}') = \delta^2 e/\delta\sqrt{g(\boldsymbol{r})}\delta\sqrt{g(\boldsymbol{r}')}$. If this operator is positive definite, the solution of the HNC-EL/0 equation (4) is stable against infinitesimal perturbations

of $g(\boldsymbol{r})$. This is guaranteed if all eigenvalues λ_i in the equation

$$\int d^2r'\, K(\boldsymbol{r},\boldsymbol{r}')f_i(\boldsymbol{r}') = \lambda_i f_i(\boldsymbol{r}) \tag{9}$$

are positive. Conversely, if the lowest eigenvalue λ_0 is close to zero, the system approaches an instability. More importantly, the eigenvector $f_0(\boldsymbol{r})$ provides information about the nature of the instability as shown by our results below. The explicit form of $K(\boldsymbol{r},\boldsymbol{r}')$ is easily calculated in the HNC-EL/0 approximation. Following the notation of Ref. [56], the eigenvalue problem can be written as

$$\left[-\frac{\hbar^2}{m}\Delta + v(\boldsymbol{r}) + w_{\rm I}(\boldsymbol{r}) + \hat{W}\right] f_i(\boldsymbol{r}) = \lambda_i f_i(\boldsymbol{r}), \tag{10}$$

where the $\hat{W}$ operator is defined as

$$\hat{W} f_i(\boldsymbol{r}) = \rho_0 \int d^2r'\, \sqrt{g(\boldsymbol{r})}\, W(\boldsymbol{r}-\boldsymbol{r}')\sqrt{g(\boldsymbol{r}')} f_i(\boldsymbol{r}'). \tag{11}$$

W is given in in momentum space as

$$W(\boldsymbol{k}) = -\frac{\hbar^2 k^2}{m}\left(1 - \frac{1}{S(\boldsymbol{k})^3}\right).$$

Since we only need the lowest eigenvalue to assess the stability, we solve Eq. (10) by imaginary time propagation (see Appendix A for details).

III. ENERGY AND STABILITY

In the liquid phase, as opposed to the gas phase, a system is self-bound: the energy per particle is negative and attains its minimum at an equilibrium density $\rho_{\rm eq}$. Furthermore, below the spinodal density a homogeneous liquid becomes unstable against long wavelength density fluctuations and then breaks into droplets. In this section we analyze the ground-state energy for various short-range repulsion strengths $C_{\rm h}$, dipole tilt angles θ, and densities ρ_0 in order to check whether the system is in a liquid phase or in a gas phase. We also assess the stability against density fluctuations. Instead of reaching a spinodal instability typical of isotropic liquids, we find a transition to a density wave in the y direction, i.e., a stripe phase.

We first fix $C_{\rm h} = 0.33r_0$ and vary the tilt angle between $\theta = 1.02$ and $\theta = 1.16$. The results are depicted in Fig. 2, where we show the energy per particle $e(\rho_0)$ as a function of the density. In each case we start the calculation at a large density and solve Eq. (4) iteratively. The resulting pair distribution function is then used as an input to solve the same equation at a lower density, which ensures rapid numerical convergence. We repeat this either until reaching zero density or until we do not find a stable solution at nonzero density. Depending on the tilting angle θ, three different cases can occur, corresponding to three different phases: a gas, a homogeneous liquid, or a striped liquid.

For $\theta \leqslant 1.04$ the energy per particle is positive and approaches zero as $\rho \to 0$ where it attains its minimum value $e = 0$. The system is then in a gas phase and the corresponding pressure is always positive. Beyond $\theta = 1.04$ the system enters a different phase where the energy per particle e becomes negative as the density is lowered. The system is self-bound

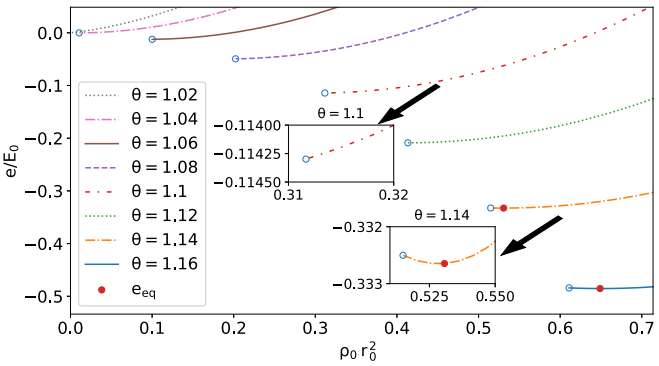

FIG. 2. Energy per particle $e(\rho_0)$ as a function of the density ρ_0 for $C_{\rm h} = 0.33r_0$ and $\theta = 1.02$–1.16. The last converging point at the lowest density in each curve is marked with a blue open circle, and the equilibrium energy $e_{\rm eq}$ is marked with a red solid circle. The insets show a magnification of the result for $\theta = 1.10$ and 1.14, which illustrates the behavior of the equation of state near the stripe phase.

and thus in a liquid phase. However, as long as $\theta \leqslant 1.12$, the calculation ceases to converge before $e(\rho_0)$ attains a minimum; the density $\rho_{\rm c}$ where this happens is indicated with open blue circles in Fig. 2. The inset for $\theta = 1.1$ shows this more clearly, where one can see that the liquid phase stops being stable before reaching a homogeneous equilibrium density $\rho_{\rm eq}$. The homogeneous HNC-EL/0 equations are know to cease to converge at a continuous phase transition [37,50]. In the following we show that the dipolar system undergoes a transition to a self-organized stripe phase where the density exhibits a spatial modulation.

Figure 3 shows the static structure factor $S(k_x = 0, k_y)$ along the y direction, for $\theta = 1.08$ and $C_{\rm h} = 0.33r_0$, and densities spanning the range from $0.2023/r_0^2$ to $1/r_0^2$. A pronounced peak grows as the density approaches a critical value of $\rho_{\rm c} = 0.2023/r_0^2$, thus signaling increasing spatial ordering between pairs of dipoles in the y direction. This suggests a self-organized long-range order below $\rho_{\rm c}$, where homogeneous HNC-EL/0 does not converge anymore. The same behavior was observed in Ref. [37], except that here the

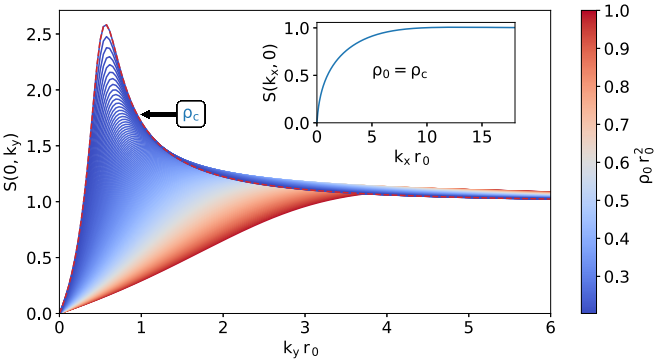

FIG. 3. Static structure factor $S(0, k_y)$ for $\theta = 1.08$ and $C_{\rm h} = 0.33r_0$ as a function of k_y. As the density (color coded) is lowered approaching a critical density of $\rho_{\rm c} = 0.2023/r_0^2$, a large peak develops. $S(k_x, 0)$, shown in the inset, is almost independent on ρ_0 and does not develop a peak.

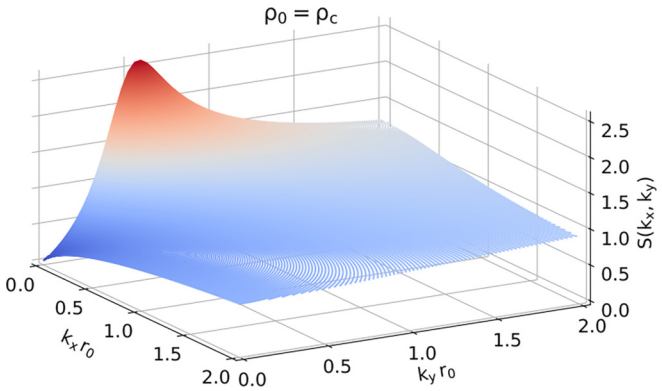

FIG. 4. Static structure factor $S(k_x, k_y)$ for $\theta = 1.08$ and $C_h = 0.33r_0$ at the critical density $\rho_c = 0.2023/r_0^2$.

density is 3 orders of magnitude lower and the dipoles are in a self-bound phase. From the position k_p of the peak in $S(k_x = 0, k_y)$, at ρ_c we can predict the wave number of the density oscillation. The pronounced peak in $S(\mathbf{k})$ is associated with a roton excitation, according to the Bjil-Feynman approximation for the dispersion relation, $\hbar\omega(k_x, k_y) = \frac{\hbar^2 k^2}{2m\, S(k_x,k_y)}$, which is expected to work well at low densities. In this way, the reported structure factor points to the emergence of a roton instability along the direction of k_y, compatible with a transition to a stripe phase. In contrast to the y direction, the structure factor in the x direction has no peak (see inset in Fig. 3), thus showing no signs of ordering in the x direction. Figure 4 shows the full $S(k_x, k_y)$ at the critical density ρ_c.

Figure 5 shows the corresponding pair distribution function $g(x, y)$ obtained as the Fourier transform of $S(k_x, k_y)$. As expected $g(x, y)$ shows a small peak along the x direction where the attractive well of the dipole-dipole interaction (Fig. 1) is deepest. Other than that, the pair distribution function is smooth. In the small range depicted, $g(x, y)$ has little structure along the y direction, and the oscillations in $g(0, y)$ that lead to the peak in $S(0, k_y)$ cannot be seen.

The emergence of a peak in the static structure factor along the y direction is thus a strong indicator for the transition to a stripe phase. A more rigorous stability analysis explained above leads to the same conclusion, as illustrated

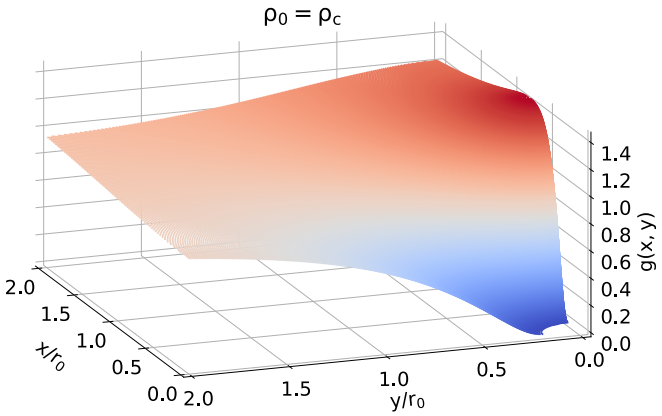

FIG. 5. Pair distribution function $g(x, y)$ for $\theta = 1.08$ and $C_h = 0.33r_0$ at the critical density $\rho_c = 0.2023/r_0^2$.

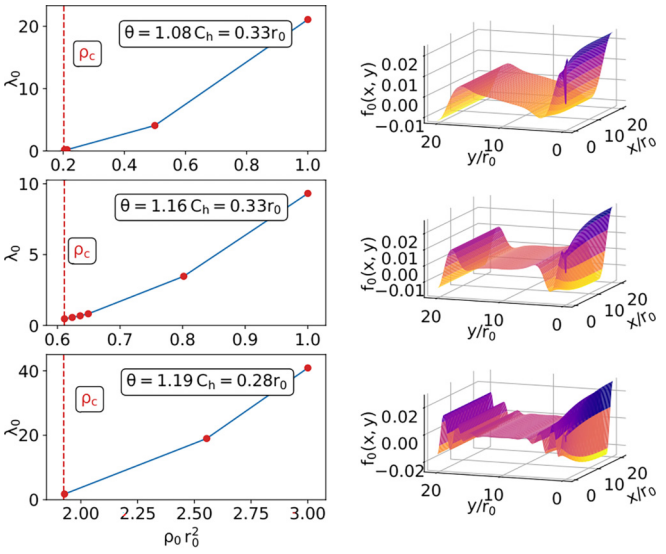

FIG. 6. Stability analysis for $C_h = 0.33r_0$ and $\theta = 1.08/1.16$ and for $C_h = 0.28r_0$ and $\theta = 1.19$. The left column shows the lowest eigenvalue λ_0 of the Hessian as a function of the density ρ_0, while the right column shows the eigenvector $f_0(\boldsymbol{r})$ at ρ_c.

in Fig. 6. The top, middle, and bottom panels correspond to ($C_h = 0.33r_0$, $\theta = 1.08$), ($C_h = 0.33r_0$, $\theta = 1.16$), and ($C_h = 0.28r_0$, $\theta = 1.19$), respectively. The left panels depict the density dependence of the lowest eigenvalue λ_0 of Eq. (10). As can be seen, λ_0 approaches zero as the density approaches ρ_c, confirming that the homogeneous phase becomes unstable in that limit. As a further confirmation we show the lowest eigenvectors $f_0(\boldsymbol{r})$ at ρ_c in the right column of the same figure. The shape of f_0 provides information about the least-stable fluctuation in $g(x, y)$, which drives the transition to a stripe phase, showing oscillations along the y direction. These oscillations are most pronounced at high densities, as seen in the bottom panel of Fig. 6. The wave number of this oscillation is the same as the wave number k_p of the peak in $S(0, k_y)$ at ρ_c (see Fig. 3). This behavior clearly signals the transition to a phase with long-range order in the y direction. Note that in all cases, the oscillation is strongly damped, which was not found for the stripe phase transition at high densities in Ref. [37], where the system is not self-bound.

When the tilting angle is increased beyond $\theta = 1.12$ while still keeping $C_h = 0.33r_0$, the energy decreases further due to the stronger attraction, but there is also a qualitative change of the shape of the equation of state shown in Fig. 2: $e(\rho_0)$ is not monotonous anymore, but reaches a minimum at a homogeneous equilibrium density ρ_{eq} before reaching the critical density ρ_c of the transition to the stripe phase. This new minimum corresponds to a self-bound homogeneous liquid state. If the system were finite, the dipoles would form a two-dimensional droplet, adjusting its radius so that the pressure inside the droplet would be zero at ρ_{eq}. When the density is lowered further the energy per particle starts increasing again, up to the point where the transition to the stripe phase takes place at ρ_c, as evidenced by the stability analysis shown in Fig. 6). The lower inset in Fig. 2 shows the result for $\theta = 1.14$, where the energy minimum at ρ_{eq} is clearly visible.

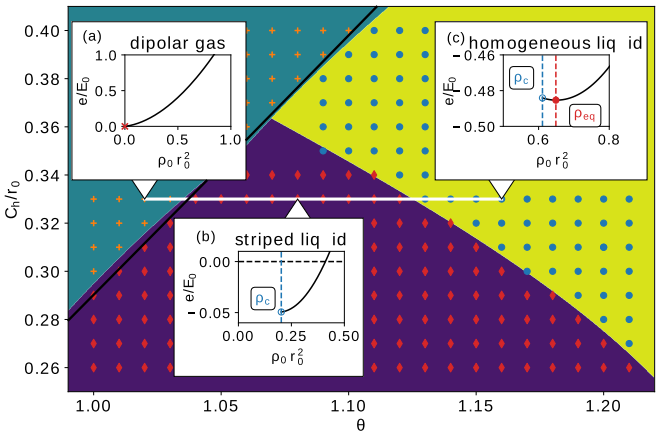

FIG. 7. Phase diagram as a function of the tilting angle θ and the short-range repulsion C_h. For a given value of $C_h = 0.33r_0$, the insets (a), (b), and (c) show a representative energy per particle $e(\rho_0)$ for $\theta = 1.02$ (gas phase), 1.08 (striped liquid phase), and 1.16 (homogeneous liquid phase). The black line indicates a resonance, below which the interaction supports a two-body bound state.

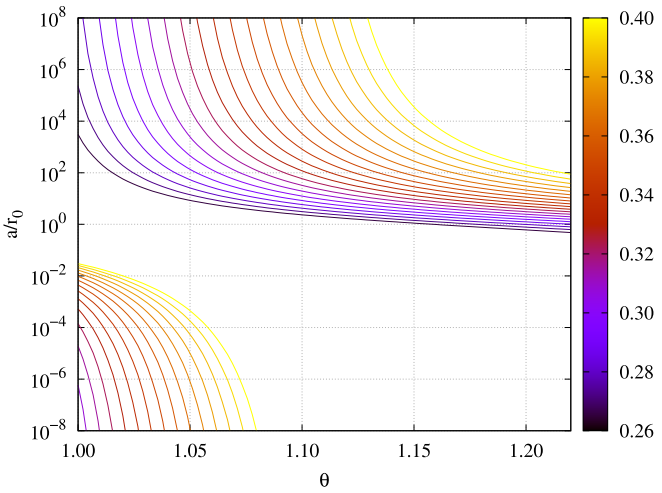

FIG. 8. Scattering length a_0 of the interaction (2) as a function of the tilting angles θ for different repulsion parameters C_h between 0.26 (black/dark) and 0.40 (yellow/bright).

IV. PHASE DIAGRAM

In order to obtain the full phase diagram, we calculate $e(\rho_0)$ for a range of θ and C_h values following the protocol described above, i.e., lowering ρ_0 from a sufficiently large value down to zero or until a homogeneous phase ceases to be stable at a finite density value ρ_c. We analyze the results in the same way as in the previous section to classify the phase into a gas phase, a striped liquid phase, and a homogeneous liquid phase. Figure 7 presents this classification, indicating the phases by different symbols, as a function of θ and C_h. Based on the grid of θ and C_h values, the boundaries between the phases were fitted using a C-support vector machine [57], and an analytic expression for those phase boundaries is given in Appendix B. In Fig. 7, a white line is drawn for the fixed repulsion parameter $C_h = 0.33r_0$ that we used in most calculations presented in the previous section. The three insets show three examples for the equation of state $e(\rho_0)$ along this line, each representing one of the phases. The points along the white line are the results based on the energies $e(\rho_0)$ shown in Fig. 2. Note that a dipolar system in 2D can also have density oscillations at very high densities $\rho_0 \sim 10^2/r_0^2$ according to Ref. [37]. However, here we focus on the formation of a stripe phase at orders of magnitude lower densities. The critical densities below which we predict a stripe phase are discussed in the following section. In the vicinity where the three phase boundaries meet, there is a gap in our grid of θ and C_h values. Predicting the correct phase, striped or not striped liquid, becomes numerically quite cumbersome in that part of the phase diagram because of the low densities involved and the shallowness of the equation of state $e(\rho_0)$ (see Fig. 2).

Figure 7 shows that, for tilting angle $\theta > 1.07$, upon increasing the repulsion strength C_h the system undergoes first a transition from a striped liquid to a homogeneous liquid, followed by a transition to a homogeneous gas. The reason is that the increasing isotropic short-range repulsion becomes dominant compared to the anisotropic dipole-dipole interaction, which is responsible for the formation of stripes. More interestingly, an increase of the tilting angle θ, and thus of the anisotropy, for a fixed short-range interaction, also drives the system to the homogeneous liquid phase, as we have discussed in Sec. III. This might seem counterintuitive at first. However, it is actually the repulsive part of the dipole-dipole interaction in the y direction causing the formation of stripes and this part of the interaction does not change with θ. At the same time the attraction in the x direction increases with increasing θ and leads to a more strongly bound system with a higher density, and the stripes merge as their wavelength decreases, where the wavelength is obtained from the wave number k_y of the peak in $S(0, k_y)$ (see Fig. 3). For example, if $C_h = 0.33r_0$ is fixed and the tilting angle is increased from $\theta = 1.08$ to $\theta = 1.16$, the wavelength decreases from $\lambda = 11.70r_0$ to $\lambda = 4.82r_0$.

At this point one may wonder whether the appearance of the three phases is universal for a dipolar system with a repulsive core, i.e., whether it depends only on the two-dimensional scattering length a_0 or changes with the model chosen for the core. The scattering length a_0 is obtained from the long-range asymptotic form of the s-wave mode of the zero-energy solution of the two-body problem, as described in Ref. [58]. The resulting values are shown in Fig. 8, where fixed C_h curves corresponding to varying θ values are shown in different colors. As it can be seen from the plot, many curves tend to diverge with decreasing angle, showing that for those C_h values the system goes through a resonance, triggering the formation of a two-body bound state. Remarkably, within the numerical uncertainties, the resonance line coincides with the boundary separating the gas phase from the homogeneous liquid and striped liquid phases in Fig. 7; it is represented by a thick black line in the same plot. As expected, in the gas phase the two-body problem shows no bound state, while in the other two phases a single two-body bound state appears for the range of C_h and θ angles considered. Since the resonance line is by definition characterized by a diverging scattering length, the transition between the gas phase and the liquid phases is universal.

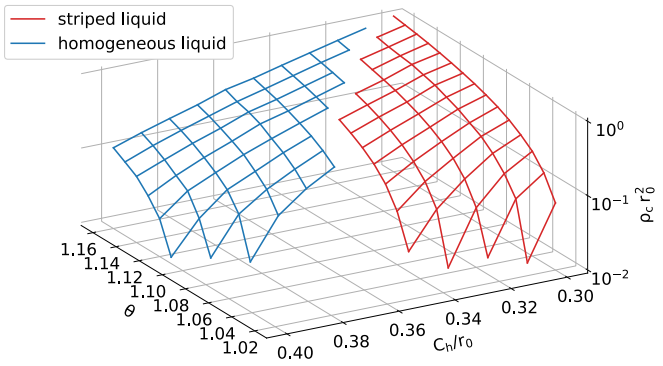

FIG. 9. Critical density ρ_c for the transition to the stripe phase as a function of θ and C_h. The red (right) and blue (left) surfaces denote the regimes of the striped liquid and the homogeneous liquid, respectively (see Fig. 7). At the border to the gas phase, ρ_c falls to zero.

The transition between the striped and the homogeneous liquid may still depend on the details of the interaction considered because the gas parameter is not small for the two liquid phases shown in Fig. 7, $\rho_0 a_0^2 > 1$ (see also the next section). In order to check whether the same phases appear and whether their phase boundaries change, we replaced the two-body repulsive core C_h^{12}/r^{12} in the interaction (2) with a different repulsive potential, namely, a $\tilde{C}_h^6/|\mathbf{r}|^6$ interaction. We find our results are robust in that we again obtain a homogeneous and a striped liquid phase. When expressed in terms of a_0, the boundary between the two phases becomes universal for smaller θ (closer to the gas phase), where the equilibrium densities are small, but it depends on the details of the model repulsion potential for larger θ, where the equilibrium densities are large (the critical densities ρ_c are shown in the following paragraph and the equilibrium densities are of similar magnitude). The details of this analysis can be found in Appendix D.

V. CRITICAL DENSITY

Figure 9 shows the critical density ρ_c for the transition to a stripe phase as a function of tilting angle θ and repulsion strength C_h, showing that ρ_c increases with increasing θ and decreasing C_h. The blue and red surfaces represent the regions of the homogeneous liquid and the striped liquid, respectively (see the phase diagram in Fig. 7). Both surfaces approach $\rho_c = 0$ as the system approaches the gas phase, seen as a sharp drop on the logarithmic scale in Fig. 9. This shows that with a proper choice of θ and C_h (or a_0), stripes can be observed in arbitrarily dilute systems. This is markedly different from previous theoretical studies of tilted dipoles in two dimensions [37], where the dipole orientation was not tilted above $\theta = \arcsin(1/\sqrt{3})$ such that the dipole-dipole interaction stays purely repulsive. In that case a stripe phase was predicted only above a critical density $\rho_c r_0^2 \sim \mathrm{O}(10^2)$. We also note that in most of the range of θ and C_h explored in this work, we have $\rho_c r_0^2 < 1$. Despite the variational nature of the calculations presented, the contribution of elementary diagrams to the energy per particle is less than 3% (see Appendix C for details), while third- or higher-order correlations are negligible in the low-density regime considered.

VI. CONCLUSION

In this work we have explored the phase diagram of a dipolar gas in two dimensions as a function of the dipole tilting angle and its short-range repulsion. We have found that this system exhibits three different phases: a gas phase, a self-bound stripe phase, and a homogeneous liquid phase with no stripes. We detected the transition to a stripe phase by monitoring a peak that emerges in the structure factor close to a critical density ρ_c that marks the phase transition. The critical density depends on the short-range repulsion and the tilting angle, and can be low enough so that it can be realized with current experimental setups. To further confirm the emergence of the low-density stripe phase we have also conducted a stability analysis based on the Hessian of the energy. Although our calculations, based on the variational HNC-EL/0 method, always assumed homogeneity, this provides strong evidence that a self-bound and striped liquid can form in a two-dimensional anisotropic dipolar Bose gas. We have also analyzed the universality of the phase diagram, checking against calculations using a different repulsive core.

While our results are compatible with a continuous transition from a homogeneous dipolar liquid phase to a striped liquid phase, more results for the latter are necessary in order to understand the properties of this phase and the nature of the phase transition, be it first or second order. For this purpose one can use a variational model that allows for density modulations, such as the inhomogeneous generalization of the HNC-EL method [59], which has been used, for example, to describe dipolar systems in quasi-2D geometries [60,61]. Alternatively one can use exact diffusion Monte Carlo methods, possibly with optimal HNC-EL solutions as guiding wave functions. We are pursuing the latter option to study the self-bound nature of two-dimensional striped dipolar systems. The melting of the striped phase at finite temperature may be studied, e.g., with path integral Monte Carlo simulations [62] or a variational density-matrix approach [63,64].

ACKNOWLEDGMENTS

We acknowledge discussions with Jürgen T. Drachta, Tilman Pfau, and J. Sanchez-Baena. F.M. acknowledges financial support by Grant No. PID2020-113565GB-C21, funded by MCIN/AEI/10.13039/501100011033, and from Secretaria d'Universitats i Recerca del Departament d'Empresa i Coneixement de la Generalitat de Catalunya, cofunded by the European Union Regional Development Fund within the ERDF Operational Program of Catalunya (project QuantumCat, Ref. No. 001-P-001644).

APPENDIX A: STABILITY ANALYSIS

Solving for the lowest eigenvalue λ_0 and associated eigenvector $y_0(x, y)$ of Eq. (10) can be done in several ways. Here

we use imaginary time propagation,

$$f_0 = \lim_{t\to\infty} \exp\left[-t\left(-\frac{\hbar^2}{m}\Delta + v(\boldsymbol{r}) + w_1(\boldsymbol{r}) + \hat{W}\right)\right]\tilde{f}, \quad \text{(A1)}$$

where $\tilde{f}$ is an initial guess with the only requirement being that it have a nonzero projection onto f_0. As usual, the time propagation is split into small time steps τ such that the exponentiation can be approximated in a suitable way. Here we use the Trotter approximation [65]. Taking the exponent of the potential functions $v(\boldsymbol{r})$ and $w_1(\boldsymbol{r})$ is trivial in r space, while the exponential of the kinetic part is carried out in momentum space. However, the integral operator $\hat{W}$ cannot be easily exponentiated. We could take the further approximation $\exp[-\tau W] \approx 1 - \tau\hat{W}$, but this would require an extremely small time step τ. Therefore, we split the integration kernel in Eq. (11) as $\hat{W} = \hat{W}_1 + \hat{W}_2 + \hat{W}_3$, with

$$\hat{W}_1 f_i(\boldsymbol{r}) = \rho_0 \int d^2r' \,[\sqrt{g(\boldsymbol{r})} - 1]W(\boldsymbol{r}-\boldsymbol{r}')\sqrt{g(\boldsymbol{r}')}f_i(\boldsymbol{r}'),$$

$$\hat{W}_2 f_i(\boldsymbol{r}) = \rho_0 \int d^2r' \, W(\boldsymbol{r}-\boldsymbol{r}')[\sqrt{g(\boldsymbol{r}')} - 1]f_i(\boldsymbol{r}'),$$

$$\hat{W}_3 f_i(\boldsymbol{r}) = \rho_0 \int d^2r' \, W(\boldsymbol{r}-\boldsymbol{r}')f_i(\boldsymbol{r}').$$

The first two terms turn out to be small because $\sqrt{g(\boldsymbol{r})} - 1$ becomes small for large r. The third term is still large but has the form of a convolution integral; hence, it can be easily exponentiated in momentum space. We obtain the following approximate imaginary time propagation operator for small time steps τ:

$$G = e^{-\frac{\tau}{2}[\frac{\hbar^2k^2}{m} + W(\boldsymbol{k})]} \, \mathcal{F} \, e^{-\frac{\tau}{2}[V(\boldsymbol{r}) + w_l(\boldsymbol{r})]}[1 - \tau(\hat{W}_1 + \hat{W}_2)]$$
$$e^{-\frac{\tau}{2}[V(\boldsymbol{r}) + w_l(\boldsymbol{r})]} \, \mathcal{F}^{-1} \, e^{-\frac{\tau}{2}[\frac{\hbar^2k^2}{m} + W(\boldsymbol{k})]},$$

where we used a symmetric form of the Trotter approximation. $\mathcal{F}$ denotes the fast Fourier transformation. For this propagator we can use a time step 2 orders of magnitude larger than for a propagator without the above splitting of $\hat{W}$ into small and large contributions.

APPENDIX B: PHASE BOUNDARIES

We use a C-support vector machine [57] to trace the boundaries of the different phases shown in Fig. 7. We have trained a classifier for each pair of the three classes ($j = 1$ for the striped liquid, $j = 2$ for the dipolar gas, and $j = 3$ for the homogeneous liquid) The classifiers have the form

$$f_j(\boldsymbol{x}) = \sum_i y_j^i \alpha_{ij} k(\boldsymbol{x}, \boldsymbol{x}^i) + b_j, \quad \text{(B1)}$$

where k is the kernel, which has been chosen to be simply

$$k(\boldsymbol{x}, \boldsymbol{x}') = (\gamma \langle \boldsymbol{x}, \boldsymbol{x}' \rangle)^d, \quad \text{(B2)}$$

where $\langle \cdots \rangle$ denotes the dot product and $\boldsymbol{x} = (\theta, C_\mathrm{h})$. For the upper panel in Fig. 7, $d = 6$, $\gamma = 3.2531$, and $b_j = \{-27.5267, 56.9545, 23.9379\}$. The dual coefficients $y_j^i\alpha_{ij}$ and the support vectors (SV) $\boldsymbol{x}^i$ are found in Table I. Each support vector is used in two classifiers so there are two dual coefficients for each $\boldsymbol{x}^i$ (columns in the upper part of Table I).

TABLE I. Dual coefficients and support vectors (SV) for the phase diagram in Fig. 7.

$y_j^i\alpha_{ij}$						
$j=1$	0	0.776	0	0	0	2.607
	6	0	6	6	2.872	0
$j=2$	0	0	−3.384			
	0.354	0.770	0			
$j=3$	0	−2.775	−6	−2.285	−6	−3.812
	−1.124	0	0	0	0	0
		θ	C_h/r_0			
SV class 1		1.14	0.32			
		1.05	0.34			
		1.11	0.34			
		1.18	0.29			
		1.19	0.28			
		1	0.29			
SV class 2		1.08	0.38			
		1.09	0.39			
		1.01	0.31			
SV class 3		1.09	0.38			
		1.13	0.33			
		1.09	0.35			
		1.16	0.31			
		1.17	0.3			
		1.21	0.27			

The phase boundaries between class j and class k are then obtained by imposing the condition

$$f_j(\boldsymbol{x}) - f_k(\boldsymbol{x}) = 0. \quad \text{(B3)}$$

The classifier was trained with tenfold cross-validation and a regularization parameter of $C = 6$, which avoids overfitting of the training data.

APPENDIX C: ELEMENTARY DIAGRAMS

We investigated the influence of elementary diagrams by calculating the energy contribution e_ele of the lowest-order elementary diagram, the four-point diagram [52]. We calculate e_ele using the pair distribution function $g(x, y)$ of the HNC-EL/0 results, i.e., from the energy optimization without elementary diagrams. This is justified if the contribution of elementary diagrams is small, otherwise elementary diagrams have to be included self-consistently in the optimization. We report the relative change in energy compared to the HNC-EL/0 result

$$\Delta e_\mathrm{ele} = \frac{e_\mathrm{ele}}{e + e_\mathrm{ele}} \quad \text{(C1)}$$

in Table II for several values of θ, C_h, and ρ_c (striped liquid) or ρ_eq (homogeneous liquid). For systems with $\rho_0 r_0^2 \lesssim 1$ the lowest-order elementary diagram only gives a small contribution and the HNC-EL/0 approximation is justified. However, for larger densities $\rho_0 r_0^2 \gtrsim 2$, our estimate for the relative energy correction Δe_ele becomes large and the elementary diagrams should be included self-consistently. In this density

TABLE II. Contribution of the elementary diagrams to the total energy $\Delta e_{\rm ele}$ in percent. The third column either gives the critical density $\rho_{\rm c}$ (rows 1, 3, 4, and 6) or the equilibrium density $\rho_{\rm eq}$ (rows 2 and 5).

θ	$C_{\rm h}/r_0$	$\rho_{\rm c/eq}\cdot r_0^2$	$\Delta e_{\rm ele}$ (%)
1.08	0.33	0.2023	0.01
1.16	0.33	0.6489	0.93
1.14	0.30	1.00	2.94
1.19	0.28	1.9245	9.31
1.21	0.27	2.4742	13.95
1.21	0.26	2.9948	20.68

regime also triplet correlations to the wave function are expected to play a significant role and should be included as well. Both triples and elementaries have been investigated for ^{4}He in the past [46].

APPENDIX D: UNIVERSALITY OF THE PHASE DIAGRAM

The majority of our calculations are based on the interaction (2) where the short-range repulsion is modeled with a $(C_{\rm h}/r)^{12}$ potential. We checked how sensitive the phase diagram (Fig. 7) is to the choice of the repulsion model and compared to results obtained with a $(\tilde{C}_{\rm h}/r)^6$ potential. For a given point $(\theta, C_{\rm h})$ in the phase diagram of Fig. 7, we chose $\tilde{C}_{\rm h}$ such that the scattering lengths a_0 of the total potential, consisting of dipole-dipole interaction and repulsion, coincided with the corresponding a_0 of the $(C_{\rm h}/r)^{12}$ repulsion model. We are particularly interested in the boundary between the homogeneous liquid phase and the striped liquid phase, indicated by solid circles and solid diamonds, respectively.

The comparison in shown in Fig. 10. For $\theta = 1.10$ the phase boundaries obtained for the two repulsion models agree. As θ increases, the phase boundaries deviate from each other. We conclude that the phase boundary between the two liquid phases tends towards a universal boundary if we are close to the gas phase (crosses). Note that this is where the critical density $\rho_{\rm c}$ for stripe formation and also the equilibrium density $\rho_{\rm eq}$ in the case of the homogeneous liquid phase are small (see Fig. 9). In the other direction (larger θ and smaller $C_{\rm h}$), these densities are on the order of unity, and the interparticle distances are on the order of $C_{\rm h}$ or $\tilde{C}_{\rm h}$. In such a case, we cannot expect universal behavior, and indeed this is what we observe.

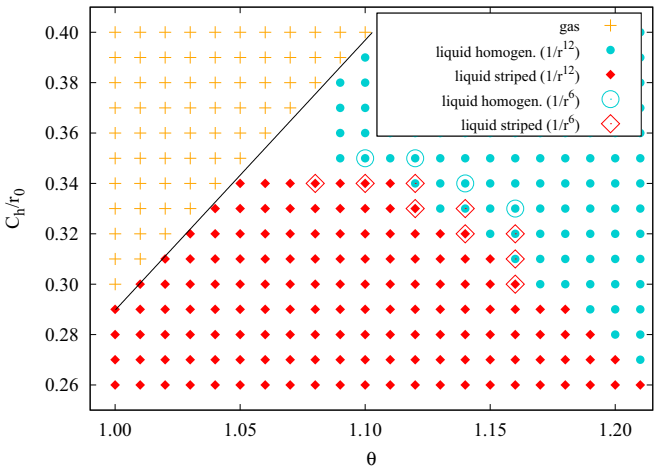

FIG. 10. Phase diagram as a function of the tilting angle θ and the short-range repulsion $C_{\rm h}$ for the $(C_{\rm h}/r)^{12}$ repulsion model. Crosses, solid circles, and solid diamonds correspond to the gas phase, the homogeneous liquid phase, and the striped liquid phase, respectively. The open circles and diamonds indicate the same liquid phases, but for calculations based on the $(\tilde{C}_{\rm h}/r)^6$ repulsion model, with $\tilde{C}_6$ adjusted such that the scattering lengths a_0 are the same. The black line indicates the boundary for two-body bound states.

The black line in Fig. 10 indicates $a_0 = \infty$; below this line the interaction supports a two-body bound state. It is evident that the boundary between the gas phase and the liquid phases is identical to the boundary for a two-body bound state, within numerical uncertainties; hence, it is universally determined by the scattering length. Note that, for all values of θ and $C_{\rm h}$ for which we studied the phase diagram, the scattering length a_0 is larger than the average particle distance $\rho_0 a_0^2 > 1$.

[1] L. Chomaz, I. Ferrier-Barbut, F. Ferlaino, B. Laburthe-Tolra, B. L. Lev, and T. Pfau, Dipolar physics: a review of experiments with magnetic quantum gases, Rep. Prog. Phys. **86**, 026401 (2023).

[2] M. Lu, N. Q. Burdick, S. H. Youn, and B. L. Lev, Strongly Dipolar Bose-Einstein Condensate of Dysprosium, Phys. Rev. Lett. **107**, 190401 (2011).

[3] H. Kadau, M. Schmitt, M. Wenzel, C. Wink, T. Maier, I. Ferrier-Barbut, and T. Pfau, Observing the Rosensweig instability of a quantum ferrofluid, Nature (London) **530**, 194 (2016).

[4] M. Schmitt, M. Wenzel, F. Böttcher, I. Ferrier-Barbut, and T. Pfau, Self-bound droplets of a dilute magnetic quantum liquid, Nature (London) **539**, 259 (2016).

[5] I. Ferrier-Barbut, H. Kadau, M. Schmitt, M. Wenzel, and T. Pfau, Observation of Quantum Droplets in a Strongly Dipolar Bose Gas, Phys. Rev. Lett. **116**, 215301 (2016).

[6] I. Ferrier-Barbut, M. Schmitt, M. Wenzel, H. Kadau, and T. Pfau, Liquid quantum droplets of ultracold magnetic atoms, J. Phys. B At. Mol. Opt. Phys. **49**, 214004 (2016).

[7] I. Ferrier-Barbut, M. Wenzel, M. Schmitt, F. Böttcher, and T. Pfau, Onset of a modulational instability in trapped dipolar Bose-Einstein condensates, Phys. Rev. A **97**, 011604(R) (2018).

[8] L. Chomaz, S. Baier, D. Petter, M. J. Mark, F. Wächtler, L. Santos, and F. Ferlaino, Quantum-Fluctuation-Driven Crossover from a Dilute Bose-Einstein Condensate to a Macrodroplet in a Dipolar Quantum Fluid, Phys. Rev. X **6**, 041039 (2016).

[9] A. R. P. Lima and A. Pelster, Quantum fluctuations in dipolar Bose gases, Phys. Rev. A **84**, 041604(R) (2011).

[10] A. R. P. Lima and A. Pelster, Beyond mean-field low-lying excitations of dipolar Bose gases, Phys. Rev. A **86**, 063609 (2012).

[11] D. S. Petrov, Quantum Mechanical Stabilization of a Collapsing Bose-Bose Mixture, Phys. Rev. Lett. **115**, 155302 (2015).
[12] C. R. Cabrera, L. Tanzi, J. Sanz, B. Naylor, P. Thomas, P. Cheiney, and L. Tarruell, Quantum liquid droplets in a mixture of Bose-Einstein condensates, Science **359**, 301 (2018).
[13] G. Semeghini, G. Ferioli, L. Masi, C. Mazzinghi, L. Wolswijk, F. Minardi, M. Modugno, G. Modugno, M. Inguscio, and M. Fattori, Self-Bound Quantum Droplets of Atomic Mixtures in Free Space, Phys. Rev. Lett. **120**, 235301 (2018).
[14] C. D'Errico, A. Burchianti, M. Prevedelli, L. Salasnich, F. Ancilotto, M. Modugno, F. Minardi, and C. Fort, Observation of quantum droplets in a heteronuclear bosonic mixture, Phys. Rev. Res. **1**, 033155 (2019).
[15] F. Wächtler and L. Santos, Quantum filaments in dipolar Bose-Einstein condensates, Phys. Rev. A **93**, 061603(R) (2016).
[16] D. Baillie, R. M. Wilson, R. N. Bisset, and P. B. Blakie, Self-bound dipolar droplet: A localized matter wave in free space, Phys. Rev. A **94**, 021602(R) (2016).
[17] R. Bombin, J. Boronat, and F. Mazzanti, Dipolar Bose Supersolid Stripes, Phys. Rev. Lett. **119**, 250402 (2017).
[18] A. Trautmann, P. Ilzhöfer, G. Durastante, C. Politi, M. Sohmen, M. J. Mark, and F. Ferlaino, Dipolar Quantum Mixtures of Erbium and Dysprosium Atoms, Phys. Rev. Lett. **121**, 213601 (2018).
[19] G. Durastante, C. Politi, M. Sohmen, P. Ilzhöfer, M. J. Mark, M. A. Norcia, and F. Ferlaino, Feshbach resonances in an erbium-dysprosium dipolar mixture, Phys. Rev. A **102**, 033330 (2020).
[20] R. N. Bisset, L. A. Peña Ardila, and L. Santos, Quantum Droplets of Dipolar Mixtures, Phys. Rev. Lett. **126**, 025301 (2021).
[21] J. C. Smith, D. Baillie, and P. B. Blakie, Quantum Droplet States of a Binary Magnetic Gas, Phys. Rev. Lett. **126**, 025302 (2021).
[22] J. Léonard, A. Morales, P. Zupancic, T. Esslinger, and T. Donner, Supersolid formation in a quantum gas breaking a continuous translational symmetry, Nature (London) **543**, 87 (2017).
[23] L. Tanzi, S. M. Roccuzzo, E. Lucioni, F. Famà, A. Fioretti, C. Gabbanini, G. Modugno, A. Recati, and S. Stringari, Supersolid symmetry breaking from compressional oscillations in a dipolar quantum gas, Nature (London) **574**, 382 (2019).
[24] Y.-C. Zhang, F. Maucher, and T. Pohl, Supersolidity around a Critical Point in Dipolar Bose-Einstein Condensates, Phys. Rev. Lett. **123**, 015301 (2019).
[25] S. M. Roccuzzo and F. Ancilotto, Supersolid behavior of a dipolar Bose-Einstein condensate confined in a tube, Phys. Rev. A **99**, 041601(R) (2019).
[26] J. Hertkorn, J.-N. Schmidt, F. Böttcher, M. Guo, M. Schmidt, K. S. H. Ng, S. D. Graham, H. P. Büchler, T. Langen, M. Zwierlein, and T. Pfau, Density Fluctuations across the Superfluid-Supersolid Phase Transition in a Dipolar Quantum Gas, Phys. Rev. X **11**, 011037 (2021).
[27] L. Tanzi, J. G. Maloberti, G. Biagioni, A. Fioretti, C. Gabbanini, and G. Modugno, Evidence of superfluidity in a dipolar supersolid from nonclassical rotational inertia, Science **371**, 1162 (2021).
[28] L. Santos, G. V. Shlyapnikov, and M. Lewenstein, Roton-Maxon Spectrum and Stability of Trapped Dipolar Bose-Einstein Condensates, Phys. Rev. Lett. **90**, 250403 (2003).
[29] D. H. J. O'Dell, S. Giovanazzi, and G. Kurizki, Rotons in Gaseous Bose-Einstein Condensates Irradiated by a Laser, Phys. Rev. Lett. **90**, 110402 (2003).
[30] L. Chomaz, R. M. W. van Bijnen, D. Petter, G. Faraoni, S. Baier, J. H. Becher, M. J. Mark, F. Wächtler, L. Santos, and F. Ferlaino, Observation of roton mode population in a dipolar quantum gas, Nat. Phys. **14**, 442 (2018).
[31] G. Natale, R. M. W. van Bijnen, A. Patscheider, D. Petter, M. J. Mark, L. Chomaz, and F. Ferlaino, Excitation Spectrum of a Trapped Dipolar Supersolid and Its Experimental Evidence, Phys. Rev. Lett. **123**, 050402 (2019).
[32] J.-N. Schmidt, J. Hertkorn, M. Guo, F. Böttcher, M. Schmidt, K. S. H. Ng, S. D. Graham, T. Langen, M. Zwierlein, and T. Pfau, Roton Excitations in an Oblate Dipolar Quantum Gas, Phys. Rev. Lett. **126**, 193002 (2021).
[33] P. B. Blakie, D. Baillie, L. Chomaz, and F. Ferlaino, Supersolidity in an elongated dipolar condensate, Phys. Rev. Res. **2**, 043318 (2020).
[34] U. R. Fischer, Stability of quasi-two-dimensional Bose-Einstein condensates with dominant dipole-dipole interactions, Phys. Rev. A **73**, 031602(R) (2006).
[35] S. Komineas and N. R. Cooper, Vortex lattices in Bose-Einstein condensates with dipolar interactions beyond the weak-interaction limit, Phys. Rev. A **75**, 023623 (2007).
[36] M. Wenzel, F. Böttcher, J.-N. Schmidt, M. Eisenmann, T. Langen, T. Pfau, and I. Ferrier-Barbut, Anisotropic Superfluid Behavior of a Dipolar Bose-Einstein Condensate, Phys. Rev. Lett. **121**, 030401 (2018).
[37] A. Macia, D. Hufnagl, F. Mazzanti, J. Boronat, and R. E. Zillich, Excitations and Stripe Phase Formation in a Two-Dimensional Dipolar Bose Gas with Tilted Polarization, Phys. Rev. Lett. **109**, 235307 (2012).
[38] L. Tanzi, E. Lucioni, F. Famà, J. Catani, A. Fioretti, C. Gabbanini, R. N. Bisset, L. Santos, and G. Modugno, Observation of a Dipolar Quantum Gas with Metastable Supersolid Properties, Phys. Rev. Lett. **122**, 130405 (2019).
[39] F. Böttcher, J.-N. Schmidt, M. Wenzel, J. Hertkorn, M. Guo, T. Langen, and T. Pfau, Transient Supersolid Properties in an Array of Dipolar Quantum Droplets, Phys. Rev. X **9**, 011051 (2019).
[40] L. Chomaz, D. Petter, P. Ilzhöfer, G. Natale, A. Trautmann, C. Politi, G. Durastante, R. M. W. van Bijnen, A. Patscheider, M. Sohmen, M. J. Mark, and F. Ferlaino, Long-Lived and Transient Supersolid Behaviors in Dipolar Quantum Gases, Phys. Rev. X **9**, 021012 (2019).
[41] P. Ilzhöfer, M. Sohmen, G. Durastante, C. Politi, A. Trautmann, G. Natale, G. Morpurgo, T. Giamarchi, L. Chomaz, M. J. Mark *et al.*, Phase coherence in out-of-equilibrium supersolid states of ultracold dipolar atoms, Nat. Phys. **17**, 356 (2021).
[42] A. Macia, J. Boronat, and F. Mazzanti, Phase diagram of dipolar bosons in two dimensions with tilted polarization, Phys. Rev. A **90**, 061601(R) (2014).
[43] A. Macia, J. Sánchez-Baena, J. Boronat, and F. Mazzanti, Droplets of Trapped Quantum Dipolar Bosons, Phys. Rev. Lett. **117**, 205301 (2016).
[44] F. Böttcher, M. Wenzel, J.-N. Schmidt, M. Guo, T. Langen, I. Ferrier-Barbut, T. Pfau, R. Bombín, J. Sánchez-Baena, J. Boronat, and F. Mazzanti, Dilute dipolar quantum droplets beyond the extended Gross-Pitaevskii equation, Phys. Rev. Res. **1**, 033088 (2019).

[45] Y. Kora and M. Boninsegni, Patterned supersolids in dipolar Bose systems, J. Low Temp. Phys. **197**, 337 (2019).
[46] E. Krotscheck, Optimal three-body correlations and elementary diagrams in liquid ^{4}He, Phys. Rev. B **33**, 3158 (1986).
[47] E. Krotscheck, Theory of correlated basis functions, in *Introduction to Modern Methods of Quantum Many-Body Theory and their Applications*, Advances in Quantum Many-Body Theory Vol. 7, edited by A. Fabrocini, S. Fantoni, and E. Krotscheck (World Scientific, Singapore, 2002), pp. 267–330.
[48] A. Polls and F. Mazzanti, Microscopic description of quantum liquids, in *Introduction to Modern Methods of Quantum Many-Body Theory and Their Applications*, Advances in Quantum Many Body Theory Vol. 7, edited by A. Fabrocini, S. Fantoni, and E. Krotscheck (World Scientific, Singapore, 2002), p. 49.
[49] M. Hebenstreit, M. Rader, and R. E. Zillich, Dipolar bilayer with antiparallel polarization: A self-bound liquid, Phys. Rev. A **93**, 013611 (2016).
[50] C. Staudinger, F. Mazzanti, and R. E. Zillich, Self-bound Bose mixtures, Phys. Rev. A **98**, 023633 (2018).
[51] E. Feenberg, *Theory of Quantum Fluids* (Academic, San Diego, 1969).
[52] J. P. Hansen and I. R. McDonald, *Theory of Simple Liquids* (Academic, San Diego, 1986).
[53] B. E. Clements, H. Forbert, E. Krotscheck, and M. Saarela, ^{4}He on weakly attractive substrates: structure stability, and wetting behavior, J. Low Temp. Phys. **95**, 849 (1994).
[54] C. E. Campbell, R. Folk, and E. Krotscheck, Critical behaviour of liquid ^{4}He at negative pressure, J. Low Temp. Phys. **105**, 13 (1996).
[55] M. Rader, M. Hebenstreit, and R. E. Zillich, Multicomponent correlated-basis-function method and its application to multilayered dipolar Bose gases, Phys. Rev. A **95**, 033625 (2017).
[56] L. Castillejo, A. D. Jackson, B. K. Jennings, and R. A. Smith, Optimal and nearly optimal distribution functions for ^{4}He, Phys. Rev. B **20**, 3631 (1979).
[57] F. Pedregosa, G. Varoquaux, A. Gramfort, V. Michel, B. Thirion, O. Grisel, M. Blondel, P. Prettenhofer, R. Weiss, V. Dubourg, J. Vanderplas, A. Passos, D. Cournapeau, M. Brucher, M. Perrot, and E. Duchesnay, Scikit-learn: Machine learning in Python, J. Mach. Learn. Res. **12**, 2825 (2011).
[58] N. N. Khuri, A. Martin, J.-M. Richard, and T. T. Wu, Low-energy potential scattering in two and three dimensions, J. Math. Phys. **50**, 072105 (2009).
[59] E. Krotscheck, Inhomogeneous quantum liquids: Statics, dynamics, and thermodynamics, in *Microscopic Quantum Many-Body Theories and Their Applications*, Lecture Notes in Physics Vol. 510, edited by J. Navarro and A. Polls (Springer, Berlin, 1998), pp. 187–250.
[60] D. Hufnagl, R. Kaltseis, V. Apaja, and R. E. Zillich, Roton-Roton Crossover in Strongly Correlated Dipolar Bose-Einstein Condensates, Phys. Rev. Lett. **107**, 065303 (2011).
[61] D. Hufnagl and R. E. Zillich, Stability and excitations of a bilayer of strongly correlated dipolar bosons, Phys. Rev. A **87**, 033624 (2013).
[62] D. M. Ceperley, Path integrals in the theory of condensed helium, Rev. Mod. Phys. **67**, 279 (1995).
[63] B. E. Clements and C. E. Campbell, Bose quantum fluids at finite temperatures: A variational density-matrix approach, Phys. Rev. B **46**, 10957 (1992).
[64] B. E. Clements, E. Krotscheck, J. A. Smith, and C. E. Campbell, Statistical mechanics of strongly correlated Bose quantum fluids, Phys. Rev. B **47**, 5239 (1993).
[65] H. F. Trotter, On the product of semi-groups of operators, Proc. Am. Math. Soc. **10**, 545 (1959).